J. Fluid Mech. (1995), *vol.* 289, *pp.* 379–405

Wavenumber transport: scattering of small-scale internal waves by large-scale wavepackets

By DAVID L. BRUHWILER[1] AND TASSO J. KAPER[2]

[1] Grumman Research and Development Center, 4 Independence Way, Princeton, NJ 08540, USA

[2]Department of Mathematics, Boston University, 111 Cummington Street, Boston, MA 02215, USA

(Received 2 August 1994 and in revised form 29 November 1994)

In this work, we treat the problem of small-scale, small-amplitude, internal waves interacting nonlinearly with a vigorous, large-scale, undulating shear. The amplitude of the background shear can be arbitrarily large, with a general profile, but our analysis requires that the amplitude vary on a length scale longer than the wavelength of the undulations. In order to illustrate the method, we consider the ray-theoretic model due to Broutman & Young (1986) of high-frequency oceanic internal waves that trap and detrap in a near-inertial wavepacket as a prototype problem. The near-inertial wavepacket tends to transport the high-frequency test waves from larger to smaller wavenumber, and hence to higher frequency. We identify the essential physical mechanisms of this wavenumber transport, and we quantify it. We also show that, for an initial ensemble of test waves with frequencies between the inertial and buoyancy frequencies and in which the number of test waves per frequency interval is proportional to the inverse square of the frequency, a single nonlinear wave–wave interaction fundamentally alters this initial distribution. After the interaction, the slope on a log-log plot is nearly flat, whereas initially it was -2. Our analysis captures this change in slope. The main techniques employed are classical adiabatic invariance theory and adiabatic separatrix crossing theory.

1. Introduction

Resonant wave–wave interactions are ubiquitous in nature. They occur in plasmas, in shallow water, between surface waves, in the atmosphere, and in the ocean, to list a few of the many places. In this work, we focus on a class of oceanic wave–wave interactions involving small-scale waves and vigorous, large-scale, oscillating background flows. We develop a method to quantitatively analyse the wavenumber transport for the small-scale waves as they interact with the velocity field of the background flow. The method relies on ray theory as well as adiabatic separatrix crossing theory.

In order to illustrate the method's utility, we apply it directly to the idealized, ray-theoretic model formulated and studied in Broutman & Young (1986, hereinafter referred to as B&Y), for the strongly nonlinear interaction between high-frequency, short-wavelength internal waves and localized packets of progressive near-inertial waves.

B&Y focuses on groups of arbitrary – but finite – amplitude near-inertial waves. This choice of focus is motivated in part by the fact that the amplitudes of the near-inertial wave velocities observed in the ocean tend to be on the order of 20 cm s^{-1}. Thus, by allowing for large amplitudes, B&Y are able to study strong, and hence realistic, shears in the velocity field of the near-inertial wave. Their approach is complementary to that offered by the induced-diffusion approximation, which owing to the inherent assumption that only those waves with velocity close to the group velocity will resonate and interact with the near-inertial wave, is only suitable for near-inertial long waves with small-amplitude velocities, with peaks on the order of 0.1 cm s^{-1}. See McComas & Bretherton (1977) for the original treatment of the induced-diffusion approximation and, e.g., Meiss & Watson (1982) for further analysis.

The upper-ocean observations of near-inertial waves reported by Pinkel (1983) also motivated the model in B&Y. In particular, Pinkel (1983) observes that near-inertial motions are vigorous in the first few hundred metres below the surface and that only a few near-inertial-wave groups are present at any given time.

In B&Y, it is first shown that in the frame of a single, infinite progressive near-inertial wave of finite amplitude, internal waves of infinitesimal amplitude are either trapped by this background wave or propagate freely past it without interacting with it. We shall refer to a near-inertial wave as the background wave and to all higher frequency internal waves as test waves, respectively, and our analysis will be performed in the frame of the background wave. In the case of untrapped test waves, the test waves can either propagate with a group velocity that is faster than the phase velocity of the background wave, in which case their vertical wavenumber is small, or their group velocity can be smaller than the phase velocity of the background wave so that they are overtaken by its phase oscillations, in which case they have a large vertical wavenumber. Then, upon shifting attention to a localized packet of near-inertial waves, it is shown that the wavenumber of an initially freely propagating small-scale (or test) wave may be permanently altered by trapping in and subsequently detrapping from the large-amplitude background wave.

The two main conclusions of B&Y may be stated as follows. First, permanent changes in the vertical wavenumber of the test waves are larger when their group velocity (c_g) is different from, but sufficiently close to, the phase velocity (c) of the background wave than when there is exact resonance ($c_g = c$). Second, numerical observations show that, as a result of an interaction, a permanent decrease in vertical wavenumber of the internal wave appears to be more likely than an increase.

Adiabatic separatrix-crossing theory is ideally suited to quantify this wavenumber transport. There are special trajectories in the frame of the near-inertial wave that act as boundaries between the states of trapped internal waves and of freely propagating internal waves. These natural boundaries correspond to separatrices in the associated phase spaces, and the large-amplitude changes in the positions of these boundaries/separatrices are responsible for the large, permanent changes in the wavenumbers of small-scale internal waves.

The fundamental idea underlying adiabatic separatrix-crossing theory is readily illustrated on a classical nonlinear planar pendulum:

$$\ddot{q} + A \sin q = 0,$$

where q is the angle the pendulum makes with the vertical, $A = g/\ell$, g is the acceleration due to gravity, ℓ is the pendulum's length, and the dot denotes the derivative with respect to time, t, the independent variable. Orbits are either librational or rotational, and the boundaries dividing these two states are separatrices corresponding

to the infinite time motion in which the pendulum starts and returns to the inverted (unstable) equilibrium. The phase-space area enclosed by the separatrices depends on the magnitude of A.

Now, with the choice of $A = A(\tau = \varepsilon t)$, for example with $A(\tau) = A_0 \exp[-\tau^2/2]$, or any other smooth, positive, slowly varying function, one models the pendulum potential with a prescribed slowly varying amplitude. The adiabatic invariant of a trajectory can be represented as an asymptotic expansion in powers of ε, and the leading-order term is the orbit's action. See Kruskal (1962) and Henrard (1993) for the development of the general theory. By definition, the orbit's action is

$$J(h,\tau) = \oint \mathrm{d}q \quad P(q,h,\tau),$$

where the initial point on the orbit lies on the contour of the Hamiltonian $H(p,q,\tau)$ frozen at the time τ. The function $P(q,h,\tau)$, which is the solution of $H(P(q,h,\tau),q,\tau) = h(J,\tau)$, explicitly gives the momentum along this contour and $\omega_0(J,\tau) = \partial h/\partial J(J,\tau)$ is the frequency of the orbit. From this definition, the orbit's action is seen to be the phase-space area it encloses. Furthermore, the theory of the adiabatic invariant states that, as long as the ratio $\varepsilon/\omega_0(J,\tau)$ is small compared to one, the real orbit will evolve in such a way that it always stays close to a contour that has this same action. This happens despite the fact that the shape and location of these contours changes by a large amount as τ changes in time.

For example, consider an initially librating pendulum and let the area enclosed by the separatrices be a locally decreasing function of τ. As long as the area enclosed by the separatrices is larger than the orbit's action, then the theory can be applied since the frequency $\omega_0(J,\tau)$ is bounded away from zero there. However, at the time $\tau_x = \varepsilon t_x$ when the area enclosed by the separatrices equals the action of the orbit, $\omega_0(J,\tau)$ vanishes and adiabatic invariance theory breaks down, since the ratio $\epsilon/\omega_0(J,\tau)$ is infinite and the series becomes disordered. From this point on, the area enclosed by any of the contours in the librational regime is smaller than the action of our orbit, and therefore there no longer exists a contour in the librational regime for our orbit to be close to. Our orbit is forced to cross the separatrix, changing its type from librating to rotating (either clockwise or counterclockwise). Furthermore, the definition of our orbit's entire adiabatic invariant, including its leading-order term the action, must also change. τ_x is referred to as the pseudo-crossing time.

Extending the classical theory of adiabatic invariance, adiabatic separatrix-crossing theory (see Cary, Escande & Tennyson 1986 and Neishtadt 1986) states that the value of the new adiabatic invariant the orbit will have after the crossing is, to lowest order, the value of the separatrix action in the new phase-space regime evaluated at the pseudo-crossing time. The separatrix action in a given phase-space region is defined to be the action associated with the separatrix. This central result from adiabatic separatrix-crossing theory forms the basis for our analysis. In fact, we shall restrict our analysis to the lowest order, which corresponds to the limit in which our small parameter vanishes. However, we remark that in principle, one can calculate the new invariant to as high an order as desired. The $O(\varepsilon)$ corrections, which have been calculated for the general case, depend on the orbit's phase at crossing, see Cary *et al.* (1986) and Cary & Skodje (1989).

The physical mechanism which results in permanent changes in wavenumber for the internal waves of our problem has a direct analogue in the relatively simple motion of the pendulum discussed above. We begin with a pendulum that is rotating counterclockwise with some action less than the action of the separatrix at maximum

amplitude. We will assume that the amplitude is initially zero and then grows and decays as the sample function $A(\tau)$ given above. Initially, the pendulum stays in the rotational regime as the amplitude grows. Eventually, there comes a time, the (first) pseudo-crossing time, at which its action equals the area enclosed by the upper separatrix. This is the time at which its trajectory will cross the upper separatrix, and, with a newly defined action, it commences to librate and classical adiabatic invariance theory applies again. Now, after a while the amplitude of the potential decreases and so by the separatrix-crossing theory we know that the trajectory must cross a separatrix (and re-enter the rotational regime) at the second pseudo-crossing time when the area enclosed by the separatrices decreases to the value of the librating pendulum's action. Whether the final rotational state of the pendulum after detrapping is clockwise (below the separatrices) or counterclockwise (above the separatrices) depends on the phase of the trajectory at this second pseudo-crossing time. Thus, a permanent change in the rotation type of the pendulum is possible, and indeed is as likely as the 'no-change' outcome.

The analogous phenomenon arises in the dynamics of internal waves and is the mechanism responsible for permanent changes in their vertical wavenumbers. Unlike the pendulum separatrices, however, the separatrices in our model are highly asymmetric. As a result, more phase-space area gets transported across the upper separatrix than across the lower one during the interaction with a localized background wavepacket. In turn, this difference in the amount of phase-space area transported directly implies that the internal waves have a higher probability of detrapping with a lower wavenumber than with a higher wavenumber.

While we treat a specific problem in this paper, the methods and approach we use are quite general. In particular, they are applicable to any situation in which small-scale, small-amplitude waves, whether atmospheric, oceanic or laboratory, encounter vigorous large-scale undulating flows. The most striking feature of our method is that it remains valid for arbitrarily strong background flows. However, the parameters governing the structure of this background flow must either (*a*) vary slowly in time compared to the natural oscillation period of the waves within the flow, or (*b*) vary in position only on scales long compared to the wavelength of the undulations.

Some of the methods used here have been successfully applied to other problems. For example, early work on resonant wave–particle dynamics lead to quasi-linear theory, see e.g. Drummond & Pines (1964), which assumes a weak background flow and is analogous to the induced diffusion approximation. Later, Fuchs *et al.* (1985) presented numerical simulations of test particles interacting with a coherent wavepacket (directly analogous to the model developed by B&Y and used here), showing that quasi-linear theory worked well for a narrow, small-amplitude wavepacket, while in contrast a broad, large-amplitude wavepacket yielded dramatically different dynamics due to particle trapping and detrapping. This new dynamics was characterized by momentum scattering plots analogous to our figures 5 and 9. Bruhwiler & Cary (1992) used adiabatic separatrix-crossing theory to quantify the results of Fuchs *et al.* (1985); subsequently, Mora (1992) used these methods to treat particles in a relativistic wave.

A detailed separatrix-crossing analysis has also been carried out in the context of fluid particle dynamics in shear layers. Meiburg & Newton (1991) show that escape times and other mixing quantities for fluid particles in a viscously decaying vortex may be obtained using a separatrix-crossing type analysis related to that used here.

This paper is organized as follows. The Hamiltonian governing the ray-theoretic model is developed in §2. In §3, the lowest-order terms of the adiabatic invariants

of all orbits are calculated. Sections 4 and 5 contain the main results of this paper. First, the separatrix-crossing analysis is carried out. Then, the wavenumber transport and the greater likelihood of permanent decreases in vertical wavenumber of the test waves are quantified. The geometric interpretation of the trapping and detrapping probability formulae, based on adiabatic Melnikov theory, is presented in §6. Finally, in §7, the effect of relaxing various assumptions inherent in the model and extensions to multiple interactions are discussed.

Note. The quantity identified as an orbit's action here (and in the context of classical mechanical systems with finitely many degrees of freedom) is completely unrelated to the wave action. In the eikonal approximation, it is assumed that each test wave has associated with it some infinitesimal, but definite, amount of intrinsic wave action. This quantity is assumed to be invariant. By contrast, once the eikonal approximation has been made, the infinitesimal test wave is treated as a particle. The action of an orbit, or trajectory the test wave executes, is then defined in terms of quantities associated with the trajectory in the phase space, and this orbital action can change by large amounts.

2. Development of the Hamiltonian

A general derivation of the Hamiltonian function which yields the eikonal equations of motion, starting from a Hamiltonian description of the fluid flow, has been presented by Henyey & Pomphrey (1983). The resulting Hamiltonian is given by a dispersion relation:

$$H(\boldsymbol{x}, \boldsymbol{k}, T) = \hat{\omega}(\boldsymbol{x}, \boldsymbol{k}) + \boldsymbol{u}(\boldsymbol{x}, T) \cdot \boldsymbol{k}. \tag{2.1}$$

The function H is equal in value to the local frequency ω of the small-scale, high-frequency test waves which obey the eikonal equations of motion. The average position $\boldsymbol{x}$ of a given test wave is the canonical coordinate, while the central wavenumber $\boldsymbol{k} = (k_x, k_y, k_z)$ of this test wave is its conjugate momentum, and time T is the independent variable. The local frequency consists of the intrinsic frequency $\hat{\omega}$ and an advective term arising due to the background fluid velocity $\boldsymbol{u}$.

For oceanic internal waves, the intrinsic frequency satisfies the dispersion relation

$$\hat{\omega}^2(\boldsymbol{x}, \boldsymbol{k}) = \frac{N^2(z)k_h^2 + f^2 k_z^2}{k_h^2 + k_z^2}, \tag{2.2}$$

where $k_h^2 = k_x^2 + k_y^2$; N is the buoyancy or Brunt–Väisälä frequency; and f is the inertial frequency. For our analysis, we follow B&Y. In particular, we assume that N and f are constant, and we employ the midfrequency approximation, which is valid when $f^2 \ll \hat{\omega}^2 \ll N^2$. In this limit, the internal wave dispersion relation becomes

$$\hat{\omega} \approx -\frac{k_h N}{k_z}. \tag{2.3}$$

We adopt the sign convention that $\hat{\omega}$ is positive, while the vertical wavenumber k_z is negative, corresponding to upwardly propagating internal waves. Strictly speaking, (2.3) is only valid in the limit that $1 \ll |k_z|/k_h \ll N/f$; therefore, given appropriate oceanic values for N and f, the allowed range for $|k_z|$ is constrained within limits determined by the magnitude of k_h. In §7, we relax the midfrequency approximation and show that the results obtained using the full dispersion relation are similar to those presented here.

Following B&Y, we model the velocity field of the near-inertial wave packet by the function

$$\boldsymbol{u}(x, T) = u_0 g(z/2L)\{\cos[b(z - cT)]\hat{x} - \sin[b(z - cT)]\hat{y}\}. \tag{2.4}$$

The envelope function $g(z/2L)$ is a function of unit width and height; thus the wavepacket's envelope varies over the length scale L with maximum value u_0, and this envelope is assumed to be stationary (i.e. zero group velocity), which, as is explained in B&Y, is consistent with an infinite horizontal wavelength and intrinsic frequency equalling f. Furthermore, the analytical techniques we employ here are applicable for any smooth envelope function g and for any smooth field components. In this work, we choose g to be a Gaussian and the components to be cosine and sine functions mainly to have a concrete prototype. Also, with this choice, the wavepacket is localized in a general fashion, and the wave is circularly polarized. Other polarizations may be achieved by changing signs on, e.g., the y-component of $\boldsymbol{u}$.

In order to completely specify the choice of the velocity field $\mathbf{u}$ given above, we make the following additional assumptions and observations. First, the phase velocity c and the vertical wavenumber b of the wavepacket are assumed constant. Hence, we have the approximate relationship $bc \approx f$, since the wavepacket is nearly inertial. Second, following B&Y, we assume $L \approx 2\pi/b$, so that our wavepacket consists of several wave oscillations propagating within a stationary, slowly varying envelope. Third, both k_x and k_y are constants of the motion, because $\mathbf{u}$ was chosen to be independent of x and y. Hence, we may treat k_h as a parameter, rather than as a dynamical variable. In addition, we can neglect the horizontal dynamics and recover the vertical equations of motion arising from the full Hamiltonian of (2.1) with a simple one-and-a-half degree-of-freedom Hamiltonian, by removing the y-component of $\boldsymbol{u}$ and introducing a constant phase $\phi_0 = \arctan(k_y/k_x)$ in the x-component of $\boldsymbol{u}$.

Finally, we introduce non-dimensional variables:

$$t = bcT \approx fT,\ q = bz,\ m = k_z\left(\frac{c}{Nk_h}\right)^{1/2}, \tag{2.5a–c}$$

$$\tilde{\omega} = \omega\left(\frac{1}{Nk_h c}\right)^{1/2},\ \varepsilon = \frac{1}{2bL},\ \mu_0 = u_0\left(\frac{k_h}{Nc}\right)^{1/2}. \tag{2.5d–f}$$

Our m and μ_0 are the m_* and μ, respectively, of B&Y.

The appropriate Hamiltonian is

$$H(q, m, t) = -\frac{1}{m} + \mu_0 g(\varepsilon q)\cos(q - t + \phi_0), \tag{2.5}$$

where t is the independent variable, q is the dependent variable and m is the canonical momentum. The Hamiltonian function H is equal in value to $\tilde{\omega}$. This Hamiltonian is the starting point of our analysis. The dynamics of this system are determined by the two dimensionless parameters μ_0 and ε. We consider the regime where μ_0 is of order unity, while ε is small. For completeness, the Hamiltonian equations of motion are

$$\frac{\mathrm{d}q}{\mathrm{d}t} = \frac{\partial H}{\partial m}(q, m, t) = \frac{1}{m^2}, \tag{2.6a}$$

$$\frac{\mathrm{d}m}{\mathrm{d}t} = -\frac{\partial H}{\partial q}(q, m, t) = \mu_0 g(\varepsilon q)\sin(q - t + \phi_0) - \varepsilon\mu_0 g'(\varepsilon q)\cos(q - t + \phi_0). \tag{2.6b}$$

Equations (2.6) are non-dimensionalized forms of the eikonal or ray equations.

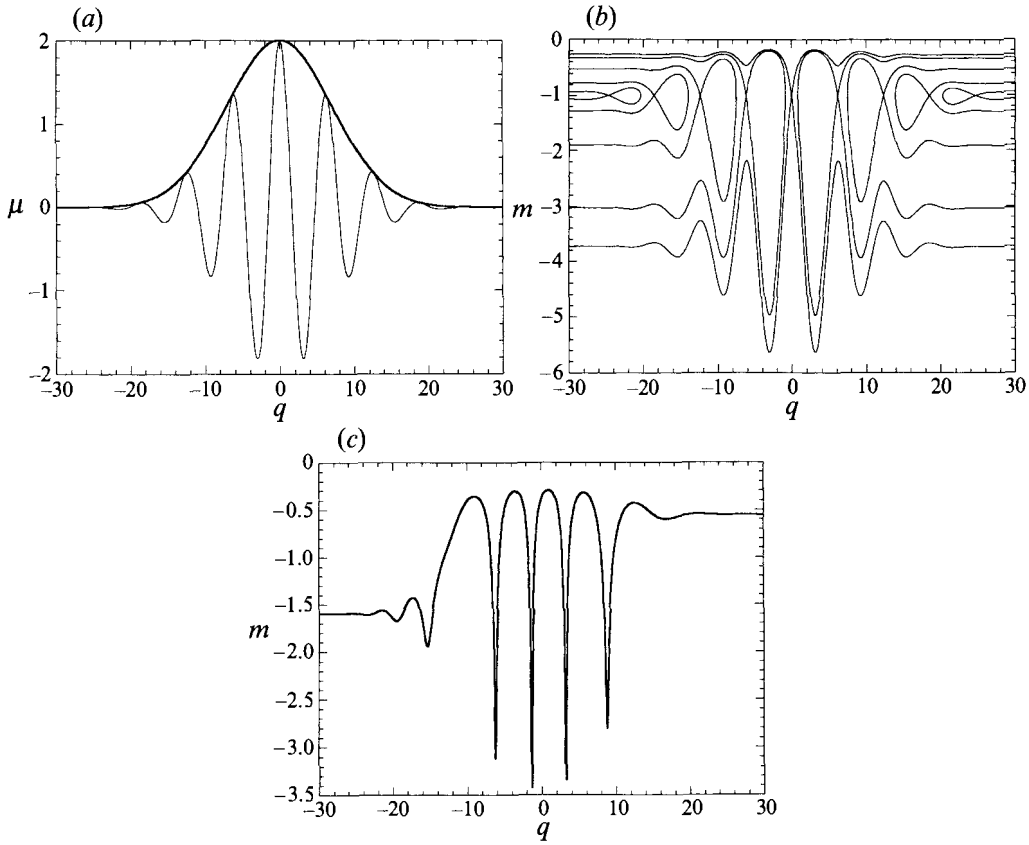

FIGURE 1. (*a*) A localized packet of background waves. The maximum wavepacket amplitude is $\mu_0 = 2.0$ and the dimensionless length parameter is $\varepsilon = 0.1$. (*b*) Snapshot of the phase-space of the Hamiltonian one would obtain by transforming into the frame moving at the phase speed of the background wave with $\mu_0 = 2.0$ and $\varepsilon = 0.1$. Only those Hamiltonian contours containing a saddle point (i.e. an unstable fixed point), are shown. (*c*) Actual trajectory (left to right) in $q - m$ space of a resonant test wave that gets scattered to a significantly smaller vertical wavenumber than it had initially. In between trapping and detrapping, it executes large-amplitude oscillations. Again, $\mu_0 = 2.0$ and $\varepsilon = 0.1$.

In figure 1(*a*), we plot the envelope of the background wavepacket $\mu_0 g(\varepsilon q)$ for $\mu_0 = 2, \varepsilon = 0.1$ and $g(\varepsilon q)$ Gaussian, and we plot the full phase oscillations, $\mu_0 g(\varepsilon q)\cos(q - t + \phi_0)$, for $t = \phi_0 = 0$. This figure is a snapshot: as time advances, the phase oscillations will move to the right at the phase velocity, which is unity in our normalized units. Since the pseudo-energy (see Broutman & Grimshaw 1988) of a test wave is given by the product of its wave action and its frequency, the contribution of the background wavepacket to the frequency of a test wave acts essentially as a source of potential energy. Thus, the dips in the phase oscillations of figure 1(*a*) are really potential wells in which test waves can become trapped. For more detailed discussions of the energy associated with test waves, we refer the reader to §2 of Broutman & Grimshaw (1988) and §3 of Henyey & Pomphrey (1983).

Figure 1(*b*) shows the contour plots in the q–m phase plane that one obtains from (2.6) by transforming to a frame moving with the phase velocity of the background wavepacket. As for figure 1(*a*), we have chosen $\mu_0 = 2, \varepsilon = 0.1$, and $t = \phi_0 = 0$. In particular, figure 1(*b*) shows only those contours which contain an unstable

equilibrium point, called an x-point or saddle point. Such contours are called separatrices, because they separate phase-space into regions in which trajectories have distinct topologies. For example, if we eliminate the time dependence from our problem, then the Hamiltonian (i.e. the frequency ω of the test wave) is a constant of the motion, and all phase-space trajectories coincide with Hamiltonian contours. In this limit, the separatrix loops seen in figure 1(*b*) contain permanently trapped trajectories, while trajectories outside these loops circle a given separatrix loop once as they are reflected by the background wavepacket. Thus, these separatrix loops correspond directly to the potential wells seen in figure 1(*a*).

For the fully time-dependent problem, this simple picture breaks down: the Hamiltonian is not a constant of the motion, phase-space trajectories do not follow Hamiltonian contours, and the separatrices seen in figure 1(*b*) are broken. However, a crude but physically useful picture of the dynamics can be drawn based on figure 1(*b*). As time progresses, the separatrix loops move from left to right at the phase velocity, so a nearly resonant trajectory (i.e. $|m|$ not too far from unity) will enter the picture from the left as some separatrix loop travels along with it, growing in time. When the separatrix loop becomes large enough, the trajectory becomes trapped in it: if the velocity of the trajectory was initially greater than unity ($|m| < 1$), then the trajectory traps into the loop from above; if its velocity was initially less than unity ($|m| > 1$), then the trajectory traps into the loop from below. Subsequently, the trajectory oscillates within the separatrix loop as it is ferried through the wavepacket. On the right side of the wave, where the loop is shrinking, the trajectory becomes detrapped. Depending on its phase, it will either detrap above or below the loop.

This trapping and detrapping process is demonstrated in figure 1(*c*) (again for $\mu_0 = 2$ and $\varepsilon = 0.1$), which shows the phase-space trajectory of a test wave that traps into a loop from below, executes large-amplitude oscillations, then detraps above the loop. In this case, the net result of the wave–wave interaction is a permanent change in the vertical wavenumber to a smaller absolute value. In order to obtain a rigorous overview of the test wave dynamics in this problem, we must transform the Hamiltonian into a form where adiabatic invariance theory can be applied; this is done in the next section.

3. Adiabatic invariance theory

Adiabatic invariance theory (Kruskal 1962 and Henrard 1993) is useful in the limit that resonant test waves execute many oscillations when traversing the background wavepacket, because it allows one to average over these fast oscillations, thus simplifying the analysis. An equivalent statement is that the theory requires variations in the envelope of the localized background wave, as perceived by a trapped trajectory, to be slow relative to the bounce time in the wave. Thus, for adiabatic theory to be applied, the Hamiltonian must be a slow function of the independent variable, usually the time. In contrast, our Hamiltonian has its slow variation in the spatial variable q, as is indicated formally by the dependence of the background wave envelope on εq, where ε is small. Therefore, we first transform to a new Hamiltonian where q is treated as the independent variable, then we proceed to calculate the adiabatic invariant.

3.1. *Preliminary transformations of the Hamiltonian*

We treat q as the independent variable simply by reversing the roles of the two conjugate pairs (q, m) and $(t, -H)$ (see e.g. Percival & Richards 1982). The negative of

the Hamiltonian, which we denote by the symbol $\tilde{\omega}^-$ in order to emphasize its new role, becomes the new momentum and t its conjugate variable. Physically, $-\tilde{\omega}^-$ is the non-dimensionalized frequency of the test wave. After this role reversal, the negative of the vertical wavenumber serves as the new Hamiltonian. Hence, we denote it by H_m and we have $H_m = -m$.

The functional form of this new Hamiltonian,

$$H_m(t, \tilde{\omega}^-, q) = -\frac{1}{\tilde{\omega}^- + \mu_0 g(\varepsilon q)\cos(q - t + \phi_0)}, \tag{3.1}$$

is obtained by solving the equation $H(q, -H_m, t) = -\tilde{\omega}^-$ for H_m. Again, adiabatic theory requires that the Hamiltonian depends on the independent variable (here q) only on the slow scale and not on the fast scale, while the Hamiltonian (3.1) has its q variation both in the slowly varying amplitude function $g(\varepsilon q)$ and in the rapidly varying phase ($q - t + \phi_0 \equiv \xi$). A canonical transformation making the phase ξ the new dependent coordinate eliminates this fast variation in q. We achieve the transformation from old variables $(t, \tilde{\omega}^-, q)$ to the new variables $(\xi, \tilde{\omega}, q)$ with a generating function of the second kind (see e.g. Percival & Richards 1982):

$$F_2(t, \tilde{\omega}, q) = (q - t + \phi_0)\tilde{\omega}, \tag{3.2}$$

which depends on the old coordinate t and the new momentum $\tilde{\omega}$, as well as the independent variable q.

The new coordinate is $\xi = \partial F_2/\partial\tilde{\omega} = q - t + \phi_0$, as desired. (Our ξ differs by a factor of 2π from the ξ of B&Y.) The relationship between the old and new momenta is given by $\tilde{\omega}^- = \partial F_2/\partial t = -\tilde{\omega}$. The new Hamiltonian is given by

$$H_\Omega(\xi, \tilde{\omega}, \varepsilon q) = H_m(t(\xi, q), -\tilde{\omega}, q) + \frac{\partial F_2}{\partial q}(t(\xi, q), \tilde{\omega}, q)$$

$$= \frac{1}{\tilde{\omega} - \mu_0 g(\varepsilon q)\cos(\xi)} + \tilde{\omega}. \tag{3.3}$$

This slowly varying Hamiltonian is equal in value to $\Omega \equiv \tilde{\omega} - m$, the (non-dimensionalized) absolute frequency of a test wave in the frame of the background inertial wave. This is a dimensionless form of the Ω that appears in B&Y. The Hamiltonian equations of motion are

$$\frac{\mathrm{d}\xi}{\mathrm{d}q} = \frac{\partial H_\Omega}{\partial\tilde{\omega}}(\xi, \tilde{\omega}, \varepsilon q) = 1 - [\tilde{\omega} - \mu_0 g(\varepsilon q)\cos(\xi)]^{-2}, \tag{3.4a}$$

$$\frac{\mathrm{d}\tilde{\omega}}{\mathrm{d}q} = -\frac{\partial H_\Omega}{\partial\xi}(\xi, \tilde{\omega}, \varepsilon q) = \mu_0 g(\varepsilon q)\sin(\xi)\,[\tilde{\omega} - \mu_0 g(\varepsilon q)\cos(\xi)]^{-2}. \tag{3.4b}$$

Equations (3.4) are dynamically equivalent to (2.6).

Figure 2 shows contours of this transformed Hamiltonian in the new $\xi - \tilde{\omega}$ phase space, which is periodic in ξ, with period 2π. In figure 2(*a*), we have chosen $\mu = \mu_0 g(\varepsilon q) = 2$. The contours are labelled with the corresponding value of the Hamiltonian (i.e. Ω), where $\Omega 1 = \mu + 2 = 4.00, \Omega 2 = 2.96$, and $\Omega 3 = 2.15$. The contour labelled $\Omega 1$ is a separatrix. We call the phase-space region above the separatrix *region a*, and phase-space trajectories in this region are said to be *passing above*. Along all trajectories passing above, $\Omega > \mu + 2$ and $|m| < 1$ (i.e. the group velocity of the corresponding test wave is greater than the phase velocity of the background wavepacket). The region below the separatrix is called *region b*, and trajectories in this region are said to be *passing below*. For all trajectories passing

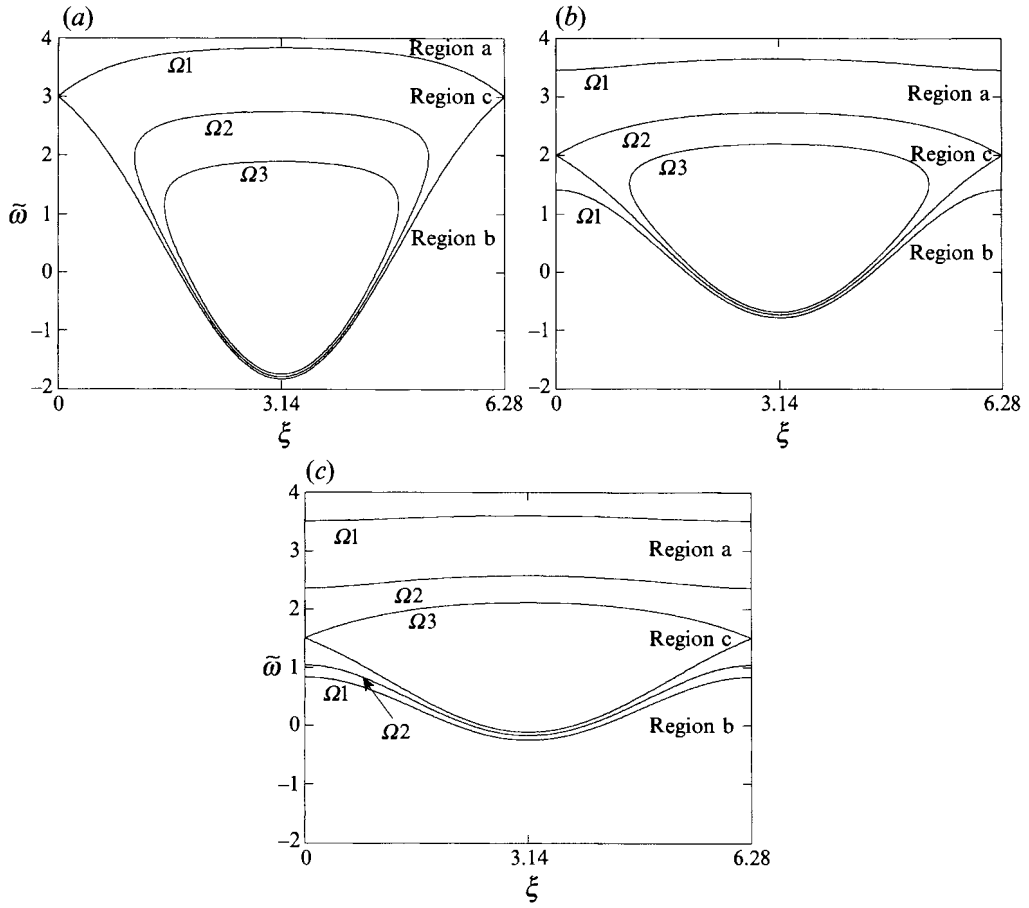

FIGURE 2. (*a*) Phase space of the transformed Hamiltonian H_Ω given by (3.3) and $\mu(\lambda) = 2.0$. The contour with $\Omega = \Omega 1 = 4.0$ defines the separatrices, while the contours $\Omega 2 = 2.96$ and $\Omega 3 = 2.15$ represent trapped trajectories. Region a lies above the upper separatrix, region b below the lower separatrix, and region c inside. (*b*) Phase space of the transformed Hamiltonian H_Ω given by (3.3) but this time with $\mu(\lambda) = 1.0$. Also, $\Omega 1 = 3.86$, $\Omega 2 = 3.0$ and $\Omega 3 = 2.15$, where the middle contour defines the separatrices. (*c*) Phase space of the transformed Hamiltonian H_Ω given by (3.3) with $\mu(\lambda) = 0.5$. Also, $\Omega 1 = 3.84$, $\Omega 2 = 2.9$ and $\Omega 3 = 2.5$, where this time the latter contour defines the separatrices.

below, $\Omega > \mu + 2$ and $|m| > 1$. Finally, we call the phase-space region inside the separatrix *region c*, and trajectories in this region are said to be trapped. For trapped trajectories, $\Omega < \mu + 2$ and $|m| - 1$ changes sign periodically as the corresponding test wave oscillates within the potential well.

In figure 2(*b*), for which we have chosen $\mu = 1$, we show three new Hamiltonian contours, again labelled $\Omega 1, \Omega 2$, and $\Omega 3$. For reasons which will become clear in §3.2 and §5 below, we have chosen these values of Ω such that corresponding contours in figures 2(*a*) (as well as 2*c*) enclose the same phase-space area. For example, the two contours labelled $\Omega 3$ in figures 2(*a*) and 2(*b*), although they have different shapes, enclose the same amount of phase-space area. Likewise, the contour labelled $\Omega 2$ in figure 2(*b*), which is a separatrix, encloses the same phase-space area as does the corresponding contour in figure 2(*a*), which is *not* a separatrix. Finally, the

two contours in figure 2(*b*) labelled $\Omega 1$, along both of which the Hamiltonian is equal to $\Omega = \Omega 1$, enclose between them the same amount of phase-space as is contained within the separatrix of figure 2(*a*). It is very important to note that the correspondingly labelled contours in figures 2(*a*) and 2(*b*) do not have the same values of Ω: in figure 2(*b*), we have $\Omega 1 = 3.86, \Omega 2 = \mu + 2 = 3.00$, and $\Omega 3 = 2.51$.

Figure 2(*c*) is a similar plot, for which $\mu = 0.5$. The separatrix, labelled $\Omega 3$, contains the same phase-space area as do the contours labelled $\Omega 3$ in figures 2(*a*) and 2(*b*). The area between the two contours labelled $\Omega 2$ is equal to the area enclosed within the separatrix of figure 2(*b*), and the area between the two contours labelled $\Omega 1$ is equal to the area enclosed within the separatrix of figure 2(*a*). For this figure, $\Omega 1 = 3.84, \Omega 2 = 2.90$, and $\Omega 3 = \mu + 2 = 2.50$.

If we eliminate the slow dependence of the background wavepacket on q (i.e. we have an infinite wavetrain), then the Hamiltonian (i.e. the absolute frequency Ω of any given test wave) is a constant of the motion, and all phase-space trajectories coincide with Hamiltonian contours. In this limit, the separatrices of figure 2 contain permanently trapped trajectories, while trajectories passing above advance continuously to the right, and trajectories passing below move to the left, as described in the Introduction.

For the full problem, this simple picture breaks down: the Hamiltonian is not a constant of the motion, phase-space trajectories do not follow Hamiltonian contours, and the separatrix is broken. However, separatrix-crossing theory uses the concept of a well-defined separatrix (which strictly exists only in the limit $\varepsilon \to 0$) for small but finite values of ε. In this dynamical picture, as a nearly resonant trajectory interacts with the background wavepacket, the separatrix will grow to some maximum size, which is governed by the maximum wave amplitude μ_0, then shrink again and disappear. When the separatrix becomes large enough, the trajectory traps: if the group velocity of the associated test wave was initially smaller than the phase velocity of the background wavepacket, then the trajectory traps into the separatrix from below; otherwise, it traps in from above. Subsequently, the trajectory oscillates within the separatrix as it is ferried through the wavepacket. On the other side of the background wavepacket, as the separatrix is shrinking, the trajectory detraps. Depending on its phase, it will either detrap above or below.

This trapping and detrapping process is demonstrated in figure 3, which shows the phase-space trajectory of a test wave that traps in from below, executes large-amplitude oscillations, then detraps above. This is the same trajectory as was shown above in figure 1(*c*), but here we are showing it in the transformed phase space. In this case, the net result of the wave–wave interaction is a permanent increase in the test wave frequency (or pseudo-energy), which corresponds to a permanent reduction in the absolute value of the vertical wavenumber. In the next subsection, we calculate the adiabatic invariant and discuss how and when trapping and detrapping of a trajectory occurs.

3.2. *Calculation of the adiabatic invariant*

Given a Hamiltonian that varies slowly with its independent variable, such as $H_\Omega(\xi, \tilde{\omega}, \lambda \equiv \varepsilon q)$ with $\varepsilon \ll 1$, there exists an adiabatic invariant, see Kruskal (1962) and Henrard (1993), which can be written as a power series in ε. The lowest-order term in this series, commonly called the action and denoted here by J, is the loop

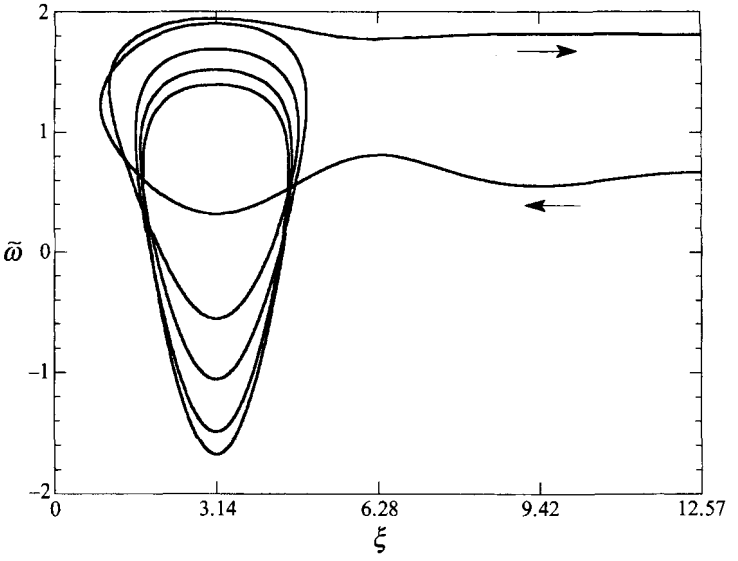

FIGURE 3. The trajectory of the same resonant test wave shown in figure 1(*c*) but now seen in the ξ–$\tilde{\omega}$ phase space of the transformed system.

integral of the canonical momentum around a phase-space trajectory:

$$J(\Omega, \lambda) \equiv \oint \mathrm{d}\xi \;\; \tilde{\omega}(\Omega, \lambda, \xi), \tag{3.5}$$

where Ω (i.e. the value of the Hamiltonian) and λ (i.e. q, the average vertical position of the test wave within the envelope of the background near-inertial wave) are held constant during the integration. The integral is evaluated in the direction of test wave motion.

The functional form of the canonical momentum, which is the (non-dimensionalized) frequency of the test wave,

$$\tilde{\omega}_{\pm}(\Omega, \lambda, \xi) = \tfrac{1}{2}\left[\Omega + \mu(\lambda)\cos(\xi)\right] \pm \left(\tfrac{1}{4}\left[\Omega + \mu(\lambda)\cos(\xi)\right]^2 - \left[1 + \Omega\mu(\lambda)\cos(\xi)\right]\right)^{1/2} \tag{3.6}$$

is obtained by solving the equation $H_{\Omega}(\xi, \tilde{\omega}_{\pm}, \lambda) = \Omega$ for $\tilde{\omega}_{\pm}$, where $\mu(\lambda) \equiv \mu_0 g(\lambda)$. We note that $\tilde{\omega}_{\pm}(\Omega, \lambda, \xi)$ is equal in value to the Hamiltonian we started out with, $H(q, m, t)$ of (2.5), but it appears in a new role with a new functional form.

Since the phase space trajectory of a test wave that is trapped within the sinusoidal oscillations of the background wavepacket contains loops, the function $\tilde{\omega}_{\pm}$ has branches. The upper branch $\tilde{\omega}_{+}$ corresponds to a test wave with an instantaneous vertical group velocity greater than the phase velocity of the background wavepacket ($|m| < 1, \xi$ increasing in time). In contrast, the lower branch $\tilde{\omega}_{-}$ corresponds to a test wave with an instantaneous vertical group velocity less than the phase velocity of the background wavepacket ($|m| > 1, \xi$ decreasing in time).

The action for trajectories passing above, denoted by J_a, is calculated by evaluating the integral of (3.5) from 0 to 2π, using $\tilde{\omega}_{+}$. The action for trajectories passing below, denoted by J_b, is calculated by evaluating this integral from 2π to 0, using $\tilde{\omega}_{-}$:

$$J_{a,b}(\Omega,\lambda) = \pm\pi\Omega + ((\Omega+\mu-2)(\Omega-\mu+2))^{1/2}$$

$$\times\left[E(k) - \frac{\Omega+\mu+2}{\Omega+\mu-2}K(k) + \frac{2\Omega(\Omega+\mu+2)}{(\Omega+\mu-2)(\Omega-\mu+2)}\Pi\left(\frac{2\mu}{\Omega-\mu+2},k\right)\right] \quad (3.7)$$

where

$$k(\Omega,\lambda) \equiv \left(\frac{8\mu}{(\Omega+\mu-2)(\Omega-\mu+2)}\right)^{1/2},$$

and + is used for J_a and − for J_b. The action for trapped trajectories, denoted by J_c, is calculated by performing a loop integral, using both branches of $\tilde{\omega}_{\pm}$. For reasons involving the behaviour of elliptic integrals, J_c has two functional forms; the first is denoted by J_{c1}, while the second, which is required only when $\mu(\lambda) - \Omega > 2$, is denoted by J_{c2}:

$$J_{c1}(\Omega,\lambda) = 4(2\mu)^{1/2}$$

$$\times\left[E(k^{-1}) + \frac{(\Omega+2)(\Omega-\mu-2)}{4\mu}K(k^{-1}) - \frac{\Omega(\Omega-\mu-2)}{4\mu}\Pi\left(\frac{\Omega+\mu-2}{2\mu},k^{-1}\right)\right], \quad (3.8a)$$

$$J_{c2}(\Omega,\lambda) = 2((\Omega+\mu+2)(-\Omega+\mu+2))^{1/2}$$

$$\times\left[E(k') + \frac{4}{\Omega-\mu-2}K(k') - \frac{8\Omega}{(\Omega+\mu+2)(\Omega-\mu-2)}\Pi\left(\frac{\Omega+\mu-2}{\Omega+\mu+2},k'\right)\right] \quad (3.8b)$$

where

$$k'(\Omega,\lambda) \equiv \left(\frac{(\Omega+\mu-2)(\Omega-\mu+2)}{(\Omega+\mu+2)(\Omega-\mu-2)}\right)^{1/2},$$

and the λ-dependence arises only through $\mu(\lambda)$, and we caution that the prime does not signify a derivative. The functions $K(k), E(k)$, and $\Pi(\alpha^2,k)$ are complete elliptic integrals of the first, second and third kind, respectively, see Byrd & Friedman (1954). Equations (3.7) and (3.8) were required to make figure 2(a–c) and figure 4.

There is a simple geometric interpretation for $J_c(\Omega,\lambda)$: for any given value of $\mu(\lambda)$, it is the phase-space area enclosed by a Hamiltonian contour of value Ω, where Ω is the current value of the absolute frequency for the trajectory of interest. The meaning of this statement becomes clearer upon consideration of figure 2. We consider a trajectory initially close to the contour labelled $\Omega 3$ in figure 2(*a*), when $\mu(\lambda) = 2$. We then suppose that $\mu(\lambda)$ decreases slowly from 2 to 1. Owing to the approximate conservation of the adiabatic invariant, we can predict that, when $\mu(\lambda) = 1$, the trajectory will be close to the contour labelled $\Omega 3$ in figure 2(*b*).

The geometric interpretation of J for passing trajectories is slightly more complicated. The phase-space area enclosed between two Hamiltonian contours in regions a and b, with the same value of Ω, such as the two contours labelled $\Omega 1$ in figure 2(*b*), is given by $J_a(\Omega,\lambda) + J_b(\Omega,\lambda)$. Conservation of $J_a(\Omega,\lambda)$ implies the following: for a passing above trajectory initially close to the upper contour labelled $\Omega 1$ in figure 2(*b*) when $\mu(\lambda) = 1$, if $\mu(\lambda)$ decreases slowly to 0.5, then we know the trajectory will be close to the upper contour labelled $\Omega 1$ in figure 2(*c*) at the final time. Conservation of $J_b(\Omega,\lambda)$ leads to analogous predictions for trajectories passing below.

We are most interested in nearly resonant trajectories, which cross the separatrix. The adiabatic invariant is discontinuous across the separatrix, because it is defined by a different integral in each of the three regions of phase space. We define the *separatrix*

action $Y(\lambda)$ to be the value of J on the separatrix. Taking the limit $\Omega \to \mu(\lambda) + 2$ of (3.7) and (3.8), we obtain

$$Y_{a,b}(\lambda) = \pm 2\pi(1 + \mu/2) + 4\left\{(\mu/2)^{1/2} + (1 + \mu/2)\arctan[(\mu/2)^{1/2}]\right\}, \tag{3.9a}$$

$$Y_c(\lambda) = Y_a(\lambda) + Y_b(\lambda), \tag{3.9b}$$

where the subscripts on Y are used to indicate the relevant region of phase space, and the λ-dependence arises through $\mu(\lambda)$. One may readily verify (3.9) by taking the limit $\Omega \to \mu(\lambda) + 2$ in (3.6) and then applying the definition of the action given by (3.5).

As long as a trajectory remains within the same region of phase space, its action is conserved to within $O(\varepsilon/{\mu_x}^{1/2})$, even if it approaches and encounters a separatrix, see Cary *et al.* (1986) and Neishtadt (1986). Here, we have used $\mu_x = \mu(\lambda_x)$, where λ_x is the pseudo-crossing time. If such a trajectory is in region α, where α can be a, b or c, and the initial value of its adiabatic invariant is J_α, then the pseudo-crossing time is defined by $J_\alpha = Y_\alpha(\lambda_x)$. If this trajectory then crosses the separatrix into region β, then the new value of its adiabatic invariant is given, to within $O(\varepsilon/{\mu_x}^{1/2})$, by $J_\beta = Y_\beta(\lambda_x)$.

The detrapping process can be visualized geometrically with the aid of figure 2. We suppose that initially $\mu(\lambda) = 2$, with a trajectory close to the contour labelled $\Omega 2$ in figure 2(*a*), then $\mu(\lambda)$ decreases slowly to 0.5. At the pseudo-crossing time λ_x, given in this case by $\mu(\lambda_x) = 1$, the trajectory is close to the separatrix shown in figure 2(*b*). Depending upon its phase, the trajectory will either detrap above the separatrix or below the separatrix. Supposing that it detraps above the separatrix, the trajectory will be found at the final time to be close to the upper $\Omega 2$ contour of figure 2(*c*). An analogous scenario occurs for trajectories that trap when the separatrix is growing.

Figure 4 shows the lowest-order adiabatic invariant (i.e. the action J plotted as a thick solid curve) for the trajectory seen previously in figure 1(*c*) and in figure 3. The transition from a trapped to a passing trajectory, or vice versa, occurs when $\Omega - 2 = \mu(\lambda)$. Both $\mu(\lambda)$ (dashed curve) and $\Omega - 2$ (dotted curve) are also plotted in figure 4. The vertical axis on the left side of the plot corresponds to J, while the axis on the right side corresponds to the other two curves. The discontinuities in J coincide with the crossing of these latter two curves. Except for these discontinuities, the action J is approximately constant (it varies only by $O(\varepsilon)$) while the background envelope, $\mu(\lambda)$, and the value of the Hamiltonian Ω both vary by large ($O(1)$) amounts. J was calculated from (3.7) and (3.8).

Adiabatic invariance theory and adiabatic separatrix-crossing theory are both asymptotic theories. The former works well for ε sufficiently small, as long as no separatrix crossings occur. The latter works well for $\varepsilon/{\mu_x}^{1/2}$ sufficiently small, where ${\mu_x}^{1/2}$ is the exponentiation rate of orbits near the saddle point at the pseudo-crossing time. For smaller values of ε, for example $\varepsilon = 0.05$, the lowest-order adiabatic invariant J was observed (in figures not shown owing to space limitations) to be more nearly constant between separatrix crossings when the background wavepacket is broader and contains more phase oscillations.

Finally, we obtain the form of the adiabatic invariant for test waves far from the background wavepacket, where the shear amplitude is vanishingly small. This calculation will prove useful in the next section. Taking the limit $\mu(\lambda) \to 0$ of (3.7) yields

$$j_a(m) = \frac{2\pi}{|m|} \qquad \text{and} \qquad j_b(m) = -\frac{2\pi}{|m|}, \tag{3.10}$$

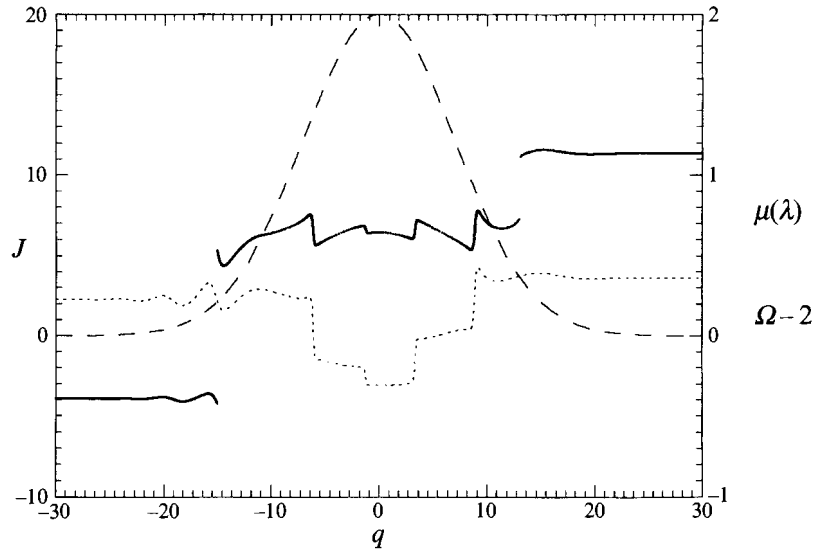

FIGURE 4. The action J of the same resonant trajectory shown in Figures 1(*c*) and 3 (solid curve, left-hand vertical axis). Also, $\mu(\lambda)$ (dashed curve) and $\Omega - 2$ (dotted curve) for the same trajectory, both using the right-hand vertical axis.

where we have used a lower-case j to indicate that this result holds only in the limit of zero shear. One may readily verify (3.10) by taking the limit $\mu \to 0$ in (3.6) and then applying the definition of the action given by (3.5). We have chosen to write j as a function of the vertical wavenumber m rather than of the absolute frequency Ω, because we are interested in calculating the permanent change in wavenumber that can occur due to separatrix crossing.

4. Wavenumber transport

As was discussed in the previous section, in the limit that $\varepsilon/\mu^{1/2}(\lambda_x) \ll 1$, the action changes only by $O(\varepsilon/\mu_x^{1/2})$, even for trajectories that approach and encounter (but do not cross) a separatrix (Cary *et al.* 1986). Given this result and our calculation of j (3.10) which was obtained from J in the limit $\mu(\lambda) \to 0$, a semi-analytic calculation (to lowest order in ε) of the final value of m for a test wave that has interacted with a coherent background wavepacket is possible. As is shown below, such a calculation provides a clear picture of the underlying structure of test wave dynamics for this problem.

Given a test wave with initial phase-space coordinates $(z_i, m_i, t_i = 0)$, with z_i chosen such that the test wave is far below the background wavepacket (i.e. zero shear), and with m_i such that a wave–wave interaction will occur, we wish to calculate the final wavenumber m_f at a later time $t_f = O(\varepsilon^{-1})$ such that the test wave is now far above the background wavepacket (i.e. again zero shear). We will assume without loss of generality that this test wave is initially below the separatrix ($|m_i| > 1$). From (3.10), the initial value of the action associated with this test wave is $J_i = j_b(m_i) = -2\pi/|m_i|$.

The action is preserved to within $O(\varepsilon)$ right up to the first encounter with the separatrix, where the test wave becomes trapped in the background wavepacket. When this separatrix crossing occurs, the local background wavepacket amplitude

is $\mu_x \equiv \mu(\lambda_x)$, and we know from (3.9) and from the constancy of the action that $J_i = Y_b(\lambda_x)$, where λ_x is determined implicitly by the relation

$$-\frac{2\pi}{|m_i|} = -2\pi(1 + \mu_x/2) + \tfrac{1}{2}Y_c(\lambda_x). \tag{4.1}$$

Since (4.1) cannot be inverted, we have only implicitly calculated $\mu_x(m_i)$ (and, hence, λ_x); this is why our calculation is only semi-analytic.

At this point the test wave is trapped, with a new adiabatic invariant given to lowest order in ε (i.e. a new action) by $Y_c(\lambda)$ of (3.9), but now with μ replaced by the μ_x just calculated in (4.1). The test wave is ferried upward through the background wavepacket, until it detraps on the other side when the amplitude has decreased from its maximum μ_0 back down to μ_x. At this point, depending sensitively on its phase, the test wave will detrap either above the separatrix or below the separatrix.

Upon detrapping, the test wave will have a third adiabatic invariant, given to lowest order by either $Y_a(\lambda)$ or $Y_b(\lambda)$ of (3.9), again with μ replaced by the μ_x we calculated in (4.1): $J_f \approx Y_a(\lambda_x)$ for detrapping above, or $J_f \approx Y_b(\lambda_x)$ for detrapping below. Since this final invariant J_f is approximately preserved as the test wave continues upward far beyond the background wave, we know also that $J_f = j(m_f)$. If the test wave detraps below the separatrix, then $m_f = m_i$ to lowest order in ε, and its vertical wavenumber is largely unchanged by the wave–wave interaction. However, if the test wave detraps above the separatrix, then an order unity change in the vertical wavenumber occurs, and the final wavenumber is given by

$$\frac{1}{|m_f|} + \frac{1}{|m_i|} = 2 + \mu_x. \tag{4.2}$$

Equation (4.2) explicitly shows that this potential change in the wavenumber increases as the initial group velocity of the test wave is moved further off resonance (i.e. as $|m_i|$ is moved further from unity and μ_x correspondingly increases), which is directly contrary to the physical picture given by the induced-diffusion approximation in the weak-interaction limit, see e.g. McComas & Bretherton (1977). B&Y previously noted this behaviour.

In figure 5, we test our understanding of the underlying test wave dynamics by comparing numerics with our semi-analytic prediction. Each plot shows the results of a numerical simulation in which an ensemble of 5×10^3 test waves, initially far beneath the background wavepacket and distributed uniformly in $-m_i$ between 0.2 and 2.9, interact once with a Gaussian wavepacket for which $\mu_0 = 2$. The final wavenumber of each test wave, $-m_f$, is plotted versus $-m_i$. The solid lines were obtained via the semi-analytic procedure described above.

Figures 5(*a*)–5(*c*) show rough agreement between theory and numerics for ε as large as 0.2 and closer agreement the smaller ε gets. We ran simulations with ε as low as 0.05. If we assume, following B&Y, that $L \approx 2\pi/b$, where we recall that L and b are the scale length and wavenumber, respectively, of the near-inertial wavepacket, then $\varepsilon \approx 1/4\pi \approx 0.08$. This corresponds to approximately eight undulations within the wavepacket, which appears to be consistent with the colour sonar plots of Pinkel (1983). The numerical data show a clear tendency for test waves with small initial wavenumber ($|m_i| < 1$) to remain at small wavenumber and for those with large initial wavenumber ($|m_i| > 1$) to move dramatically to smaller wavenumbers.

The structure in figure 5, especially in figure 5(*c*), shows distinctly the two possible fates of a test wave in the limit of small ε: either an $O(\varepsilon)$ change in vertical wavenumber, or else an order unity change in wavenumber. The 'wings' of this bird-

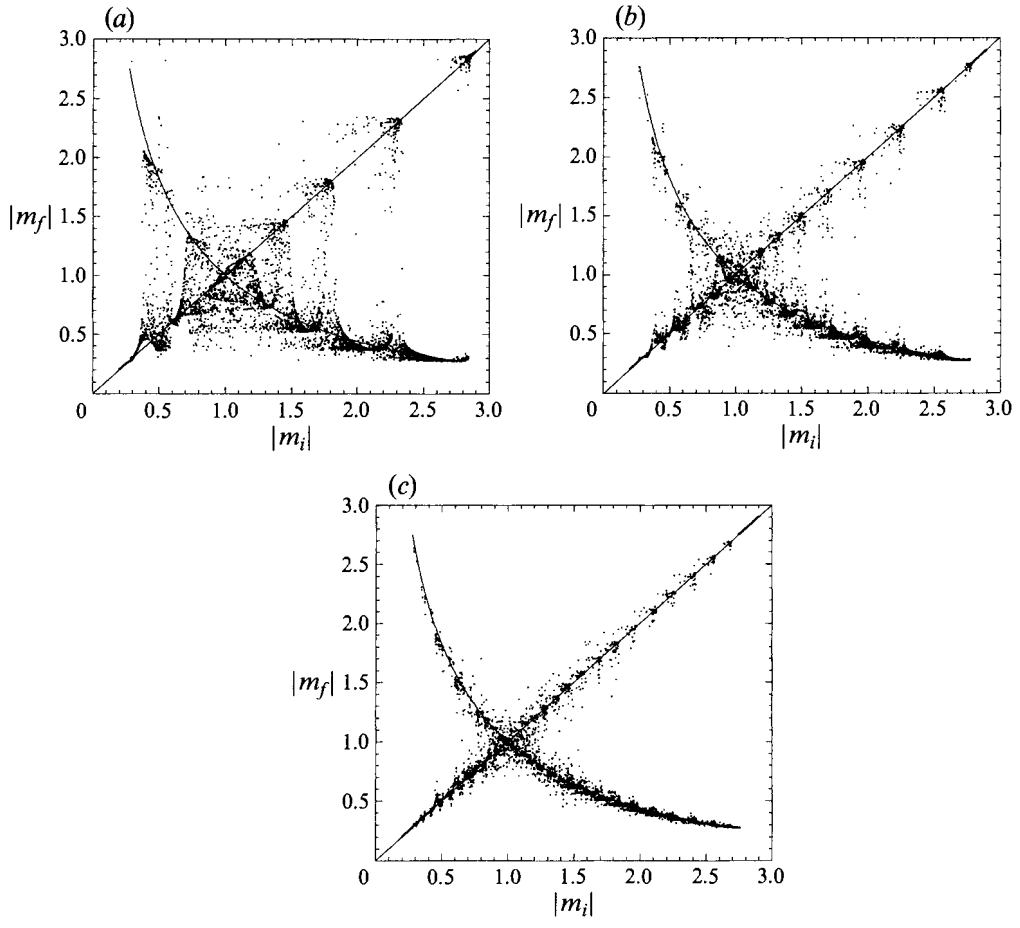

FIGURE 5. Scatter plots showing the results (in each case) of simulating 5×10^3 test waves for $\mu_0 = 2.0$ and (*a*) $\varepsilon = 0.2$, (*b*) $\varepsilon = 0.1$, and (*c*) $\varepsilon = 0.05$. In simulations with $\varepsilon < 0.05$, all of the data points fell in extremely narrow bands about the bird-like structure. In simulations with $0.5 > \varepsilon > 0.2$, the data points cover a large area, and only a few 'scrolls' were visible. In all cases, a canonical second-order leap-frog integration routine was used.

like structure connect to the 'body' at the point $-m_i = -m_f = 1$, which corresponds to exact resonance between the internal waves and the background wavepacket. As one moves further from exact resonance, the wings extend further from the body, as predicted by our analysis. However, the wings are of finite length, and those test waves that are far enough off resonance will not interact resonantly with the background wavepacket.

We can calculate the wavenumber limits beyond which these wave–wave interactions cannot occur, by equating the initial adiabatic invariant when far from the wavepacket with the separatrix action associated with the maximum wavepacket amplitude, μ_0. Doing this both above and below the separatrix yields:

$$|M_{a,b}|^{-1} = (1 + \mu_0/2) \pm \frac{1}{4\pi} Y_c(\lambda_0). \tag{4.3}$$

Test waves having an initial vertical wavenumber $|m_i| > |M_b|$ or $|m_i| < |M_a|$ will not interact resonantly with the background wave, because their phase-space trajectories

will never cross the separatrix. For this reason, the adiabatic invariant series of these non-interacting waves is preserved to all orders in ε, and the difference between m_f and m_i is zero to all orders in ε. For $\mu_0 = 2.0$, we find $|M_a| \approx 0.275$ and $|M_b| \approx 2.75$, in agreement with figure 5.

If we were to replot figure 5 for smaller values of μ_0, we would see the wings decrease in length as the range of initial m resulting in resonant wave–wave interaction decreased. This process would continue until, when μ_0 reached zero, the plot would consist of a single, continuous line of unit slope. Likewise, increasing μ_0 would increase the length of the wings.

5. Scattering to smaller wavenumber

Our analysis of the eikonal or ray equations has shown that, given an ensemble of test waves that are both initially and finally far from the background wavepacket, many of the nearly resonant test waves experience a permanent change in vertical wavenumber. We have explained the physical origin of this phenomenon and, in particular, why this potential change in wavenumber becomes larger as a given trajectory is moved further off resonance. It is evident in figure 5 that the majority of test waves emerge from the wavepacket with a final wavenumber that is smaller in absolute value than unity, the resonant wavenumber. B&Y previously noted this tendency towards transport from larger to smaller wavenumber.

In this section, we quantify this tendency. We begin by referring once more to figure 2. We suppose that $\mu(\lambda) = 2$ at the initial time, after which it decreases slowly until $\mu(\lambda) = 1$ at the final time. From the discussion in §3.2, we know that, given an ensemble of trajectories near the $\Omega 2$ contour of figure 2(*a*) at the initial time, these trajectories will be found close to the separatrix of figure 2(*b*) at the final time. Likewise, an ensemble of trajectories near the separatrix of figure 2(*a*) at the initial time will be found outside the separatrix at the final time, some of them close to the upper $\Omega 1$ contour of figure 2(*b*) and the remainder near the lower $\Omega 1$ contour.

Thus we see that the entire phase-space region between contours $\Omega 1$ and $\Omega 2$ of figure 2(*a*) is being transported through the separatrix as $\mu(\lambda)$ decreases from 2 to 1, and that finally this same phase-space area lies in between the $\Omega 2$ contour and the two $\Omega 1$ contours of figure 2(*b*). Inspection of figure 2(*b*) shows that the great majority of the expelled phase space lies above the separatrix. We conclude that for any ensemble of trapped trajectories which is randomly distributed in phase with values of Ω between $\Omega 1$ and $\Omega 2$ at the initial time, the majority of them will detrap above the separatrix. This is the physical origin of the wavenumber transport from larger to smaller absolute value. (It was shown above that trajectories passing above have vertical wavenumbers of absolute value less than unity, while those passing below have vertical wavenumbers of absolute value greater than unity.)

It has been shown for general planar adiabatic Hamiltonian systems (Neishtadt 1975; Yoder 1979; Henrard 1982, 1993; Cary *et al.* 1986) that, given an ensemble of trapped trajectories with the same action and uniformly distributed in phase, the fraction $R_a \equiv Y_a'(\lambda_x)/Y_c'(\lambda_x)$ detraps into region a, while the fraction $R_b \equiv Y_b'(\lambda_x)/Y_c'(\lambda_x)$ detraps into region b, where the prime here denotes differentiation with respect to λ:

$$R_a(\lambda) = \frac{(\pi/2)(\mu/2)^{1/2} + 1 + (\mu/2)^{1/2}\arctan[(\mu/2)^{1/2}]}{2\{1 + (\mu/2)^{1/2}\arctan[(\mu/2)^{1/2}]\}}, \tag{5.1a}$$

$$R_b(\lambda) = 1 - R_a(\lambda). \tag{5.1b}$$

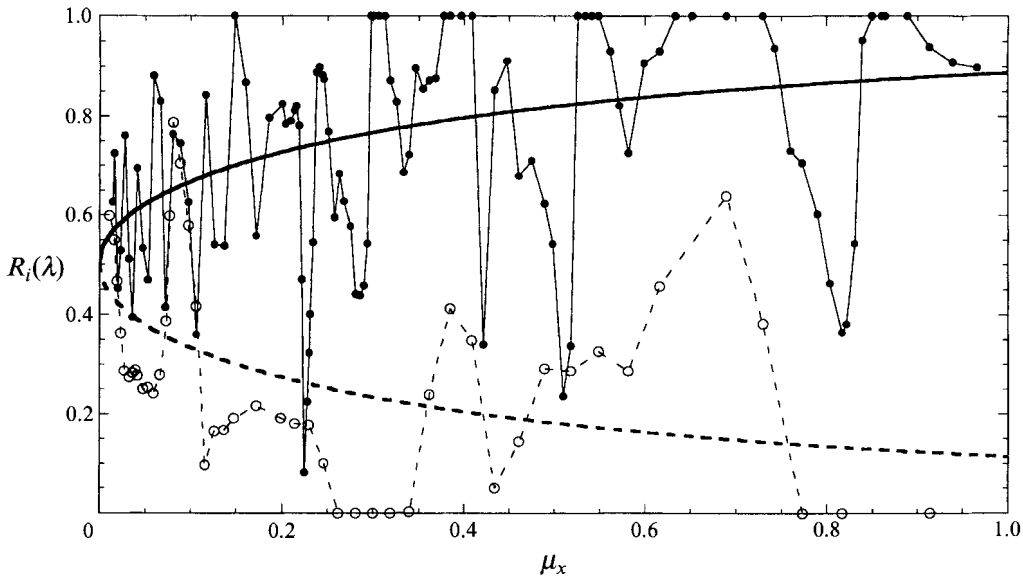

FIGURE 6. The thick solid curve is the function $R_a(\lambda)$ given by (5.1), while the thick dashed curve is $R_b(\lambda)$. The closed circles connected by thin solid lines show numerical results for $R_a(\lambda)$, with $\mu_0 = 2.0$ and $\varepsilon = 0.03$. The open circles connected by thin dashed lines show numerical results for $R_b(\lambda)$, with $\mu_0 = 2.0$ and $\varepsilon = 0.1$. Each data point is from a simulation using 1000 test waves.

These functions are plotted in figure 6.

Comparison with numerics shows oscillations about this lowest-order prediction. This occurs because, although the test wave ensembles used for the simulations were initially distributed randomly in phase, phase correlations developed between the first separatrix crossing when they trapped and the second separatrix crossing when they detrapped. There are roughly $O(1/\varepsilon)$ oscillations in the data which have $O(1)$ amplitude. See figure 6, where the the solid dots represent the probability of detrapping above in the case of $\varepsilon = 0.03$ and the open circles represent the probability of detrapping below in the case of $\varepsilon = 0.1$. Such oscillations in the detrapping fraction have been observed previously (Cary & Skodje 1989; Bruhwiler 1990; Bruhwiler & Cary 1994). Studying them in detail requires calculation of the separatrix-crossing map through first-order in ε.

6. Geometric interpretation of the detrapping probability formulae

The goal of this section is to give a geometric phase-space interpretation, based on the adiabatic Melnikov function, of the detrapping probability formulae (5.1). We show explicitly that the detrapping probabilities arise from certain ratios in the gap sizes in the broken separatrices. This geometric approach has been used by Robinson (1983) in the context of capture into resonance of satellites, and in the context of a time-dependent, two-dimensional mixing study by Kaper & Wiggins (1993). The earlier works of Neishtadt (1975), Henrard (1982), and Yoder (1979) also developed the gap-size interpretation in the context of celestial mechanics.

When $\varepsilon = 0$, the system governed by the transformed Hamiltonian (3.3):

$$H_\Omega(\tilde{\omega}, \xi, \lambda) = \frac{1}{\tilde{\omega} - \mu(\lambda)\cos(\xi)} + \tilde{\omega}$$

has a pair of unstable equilibria at $(\tilde{\omega}_f(\lambda), 0, \lambda)$ and at $(\tilde{\omega}_f(\lambda), 2\pi, \lambda)$ for each real value of λ in the three-dimensional phase space $\tilde{\omega} - \xi - \lambda$. The unions of these saddles over all real values of λ form two curves of fixed points:

$$\gamma_1 \equiv \bigcup_{\lambda\text{real}} (\tilde{\omega}_f(\lambda), 0, \lambda),$$

and

$$\gamma_2 \equiv \bigcup_{\lambda\text{real}} (\tilde{\omega}_f(\lambda), 2\pi, \lambda).$$

These curves γ_1 and γ_2 constitute normally hyperbolic invariant manifolds and are connected to each other by two-dimensional surfaces of heteroclinic orbits parametrized by the separatrix solutions $(\tilde{\omega}^h_\pm(q,\lambda), \xi^h_\pm(q,\lambda), \lambda)$. These surfaces are the unions of the stable and unstable manifolds. Finally, the normal vector to the upper/lower separatrix that is parallel to the line $\xi = \pi$ and goes through the point $a_\pm$ on the separatrix is

$$\boldsymbol{n}_\pm(a_\pm) = \left(\frac{\partial H}{\partial \xi}(a_\pm), \frac{\partial H}{\partial \tilde{\omega}}(a_\pm), \frac{\partial H}{\partial \lambda}(a_\pm) - \frac{\partial H}{\partial \lambda}(\tilde{\omega}_f(\lambda), 0, \lambda) \right).$$

We now describe the relevant structures in the system with $0 < \varepsilon \ll 1$, relating them to those of the $\varepsilon = 0$ system. First, the normally hyperbolic invariant manifolds γ_1 and γ_2 persist as slow, one-dimensional unstable orbits, which we denote $\gamma_{1,\varepsilon}$ and $\gamma_{2,\varepsilon}$, respectively. Second, the stable and unstable manifolds of these slow orbits also persist, and they contain all of the orbits that are forward and backward asymptotic in time, respectively, to $\gamma_{1,\varepsilon}$ and $\gamma_{2,\varepsilon}$. We shall denote these perturbed manifolds by $W^U(\gamma_{1,\varepsilon})$, $W^S(\gamma_{1,\varepsilon})$, $W^U(\gamma_{2,\varepsilon})$, and $W^S(\gamma_{2,\varepsilon})$. Also, for a fixed λ, we let a^u_+ and a^s_+ denote the points where $W^U(\gamma_{1,\varepsilon})$, and $W^S(\gamma_{2,\varepsilon})$, respectively, first intersect the normal vector $\boldsymbol{n}_+(a_+)$; and, similarly, a^u_- and a^s_- denote the points where $W^U(\gamma_{2,\varepsilon})$, and $W^S(\gamma_{1,\varepsilon})$, respectively, first intersect the normal vector $\boldsymbol{n}_-(a_-)$. See figure 7. On the plane λ =constant shown in figure 7, the distance between the points a^u_+ and a^s_+ is given by

$$d_+(a_+, \epsilon) = \epsilon \frac{M_+(\lambda)}{\|\boldsymbol{n}_+(a_+)\|} + O(\epsilon^2). \tag{6.1}$$

Similarly, the distance between the points a^u_- and a^s_- is given by

$$d_-(a_-, \epsilon) = \epsilon \frac{M_-(\lambda)}{\|\boldsymbol{n}_-(a_-)\|} + O(\epsilon^2). \tag{6.2}$$

Here the adiabatic Melnikov integrals are

$$M_\pm(\lambda) \equiv \int_{-\infty}^{\infty} \left[\frac{\partial H}{\partial \lambda}(\tilde{\omega}^h_\pm(q,\lambda), \xi^h_\pm(q,\lambda), \lambda) - \frac{\partial H}{\partial \lambda}(\tilde{\omega}_f(\lambda), 0, \lambda) \right] dq. \tag{6.3}$$

In the case of our model,

$$\frac{\partial H}{\partial \lambda} = \frac{\mu'(\lambda)\cos(\xi)}{(\tilde{\omega} - \mu(\lambda)\cos(\xi))^2}, \tag{6.4}$$

where $'$ denotes the derivative with respect to λ. Hence, we have

$$M_\pm(\lambda) = \mu'(\lambda) \left(\pm\pi + 2 \left(\frac{2}{\mu(\lambda)} \right)^{1/2} + 2 \arctan \left(\frac{\mu(\lambda)}{2} \right)^{1/2} \right), \tag{6.5}$$

where the coefficient in parentheses is positive for all real λ, since it is monotonically

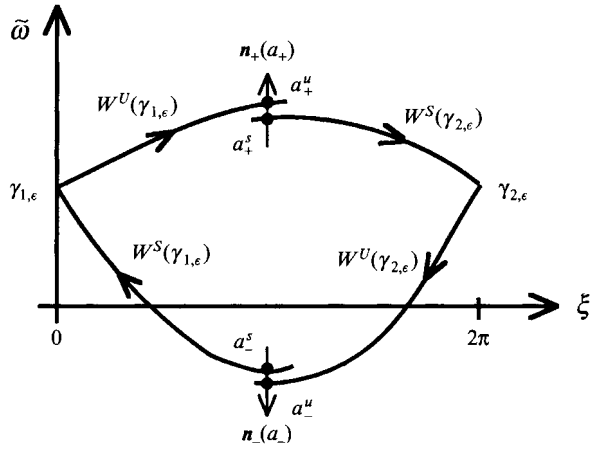

FIGURE 7. Schematic of the Melnikov splitting distance calculation performed on a plane of constant λ in §6. The distances $d_\pm \equiv \|a_\pm^u - a_\pm^s\|$.

decreasing for $\lambda < 0$, has a positive minimum at $\lambda = 0$, and is monotonically increasing for $\lambda > 0$.

Finally, we discuss the relation between the Melnikov geometric approach here and the separatrix-crossing theory used in the previous sections. Suppose that during the slow interval λ to λ_1, where λ and λ_1 are sufficiently close, the area enclosed by the separatrices decreases (the decrease below the upper separatrix, for example, being known as precisely $Y_a(\lambda) - Y_a(\lambda_1)$). Thus, since the vector field is incompressible, we know that this amount of phase-space area detraps through the upper and lower gaps from inside the separatrix region in that same interval of slow time. Keeping λ fixed and sending $\lambda_1 \to \lambda$, we obtain the relations

$$Y_a'(\lambda) = M_+(\lambda) \qquad \text{and} \qquad Y_b'(\lambda) = M_-(\lambda). \tag{6.6}$$

Formulae (6.6) relating the rate of change of the separatrix action (i.e. the rate of change of the area enclosed by the separatrix) to the adiabatic Melnikov function were established in Kaper & Wiggins (1991) and Kaper & Kovačič (1994) for general singularly perturbed two-dimensional vector fields. They were also used in the context of a time-dependent, two-dimensional mixing study in Kaper & Wiggins (1993).

These two splitting distance measurements, which represent the width of the gap between the stable and unstable manifolds as measured along the normal vectors $\boldsymbol{n}_\pm(a_\pm)$, suffice to determine the detrapping probabilities (5.1) reported in the previous section. For a fixed value of λ, the probability of detrapping above the separatrix is given to leading order by the ratio of the uppergap width $d_+(a_+, \varepsilon)$ to the sum of the two gap widths. Likewise, the probability of detrapping below the separatrix is given to leading order by the ratio of the lowergap width $d_-(a_-, \varepsilon)$ to the sum of the two gap widths.

7. Discussion

In this final section, we discuss the dramatic dynamical effect of a vigorous large-scale near-inertial wavepacket on an entire distribution of high-frequency test waves. We also discuss the effect of relaxing various assumptions in the B&Y model, and

we indicate some possible extensions of the method developed here to the case of periodic interactions.

7.1. *Evolution of a distribution of test waves*

An analysis of test wave trajectories in the eikonal approximation does not itself constitute a transport theory. Of more direct interest is the time evolution of a realistic ensemble of waves. Here, we take a step in this direction by considering the evolution of an assumed initial distribution of test waves, each wave far below the near-inertial wavepacket, which encounter the wavepacket once and are finally far above the wavepacket. The initial distribution is chosen by letting the number of test waves per unit frequency interval scale like the inverse square of the frequency, each test wave having the same horizontal wavenumber k_h.

This initial distribution is shown as a dashed line in figure 8. Also seen in figure 8 is the final distribution resulting from a numerical simulation (squares connected by dotted line) and the final distribution as predicted by our analysis (solid line). The numerical results were obtained by integrating every test wave through the wavepacket, then binning them according to their final frequency. The solid line was found via the following algorithm: (i) the initial wavenumber of each test wave was determined from the initial frequency; (ii) if this wavenumber was outside of the resonant or separatrix-crossing regime, it was left unchanged; otherwise, (iii) a potentially new wavenumber was calculated using the analysis of §4 above; (iv) the probability of detrapping from the wave with the new wavenumber or the original wavenumber were determined from (5.1); (v) a random number generator was used to decide, given these probabilities, whether or not a permanent change in wavenumber occurred; (vi) finally, each final wavenumber was converted back to a frequency, and the test waves were binned according to frequency.

Figure 8 shows that the portion of the initial distribution which lies in the resonant regime of the background wavepacket is altered dramatically. An initial slope of -2 becomes essentially flat. This result suggests that near-inertial wavepackets like those observed by Pinkel (1983) may have an observable effect on the local high-frequency internal wave spectrum. In addition, Marmorino, Rosenblum & Trump (1987) measured intense activity within near-inertial wavepackets in the upper ocean, including groups of small-scale internal waves. They suggest that similar measurements might be able to address the effect of such wavepackets on previously existing small-scale, high-frequency waves. Of course, in experimental measurements, the spectra are averaged over the entire range of frequencies so that the contribution of the inertial waves to the spectrum is included, while in our analysis this contribution is ignored. A detailed comparison between theory and numerics would require observation of the internal wave spectrum in the midfrequency regime both in the presence and in the absence of near-inertial oscillations.

Figure 8 also shows that our lowest-order (i.e. $\varepsilon \to 0$) analysis qualitatively agrees with the detailed numerical simulation. The strong oscillations seen in the numerical results arise from phase correlations and are directly related to the oscillations seen in figure 6. Although our analysis neglects these oscillations, it does capture the important effect, namely the dramatic transport of wave energy from lower to higher frequency.

Since the pseudo-energy associated with a test wave is proportional to its frequency in the eikonal approximation, we see that the near-inertial wavepacket is pumping energy into the distribution of small-scale high-frequency test waves. Although our analysis is not self-consistent, in that we neglect the effect of the high-frequency

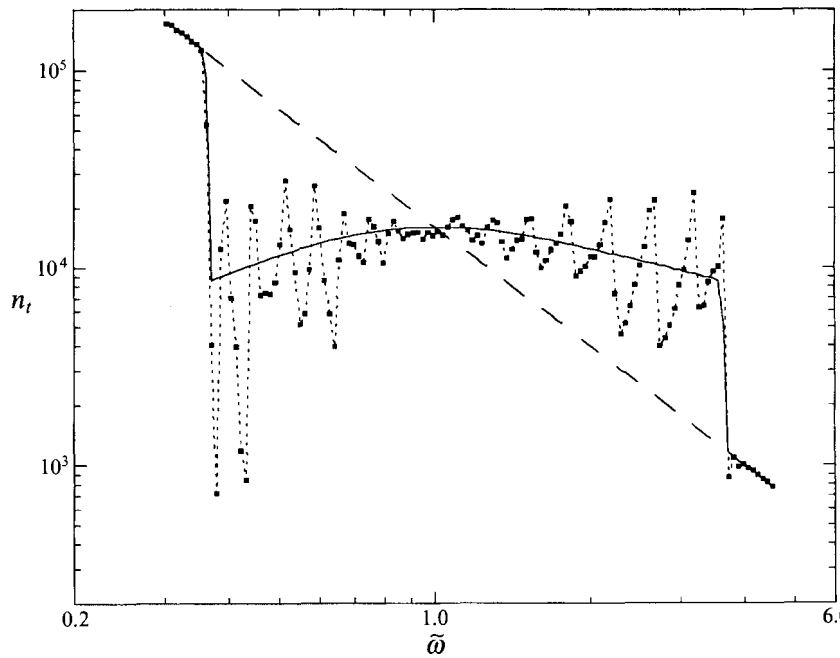

FIGURE 8. Here n_t on the vertical axis denotes the number of test waves per unit frequency interval. The dashed line represents an initial test wave distribution with a frequency spectrum of $\tilde{\omega}^{-2}$. The solid curve shows the frequency spectrum of this distribution after one interaction with the near-inertial wavepacket, as predicted by our lowest-order analysis for $\mu_0 = 2.0$. The squares connected by a dotted curve show for comparison the results of numerically integrating the same initial distribution ($\approx 5 \times 10^4$ test waves) through this near-inertial wavepacket with $\mu_0 = 2.0$ and $\varepsilon = 0.1$.

waves on the near-inertial wavepacket, it is evident from figure 8 that this nonlinear interaction would damp such a wavepacket. Broutman & Grimshaw (1988) perform a self-consistent analysis showing that a train of small trailing inertial waves is created by the interaction, and that their creation accounts for the energy balance.

We note again that our analysis throughout this work has assumed the same horizontal wavenumber k_h for all test waves. However, any realistic ensemble of internal oceanic waves would likely possess a spectrum of different values of k_h, see e.g. Munk (1981), and hence, also a spectrum of different values of the maximum dimensionless amplitude μ_0, see (2.5). Therefore, an interesting extension of the work presented here would be to model an ensemble of test waves with an appropriate spectrum of μ_0 values.

7.2. *Towards a more general model*

Here we consider the effect of abandoning the midfrequency approximation for the full internal wave dispersion relation. The test wave dynamics is found to be qualitatively the same. We also discuss the possibility of using a more general model for the near-inertial wavepacket.

When the full dispersion relation is employed, the physical mechanism of trapping and detrapping is the same as when the midfrequency approximation is used. Moreover, we again find that a larger fraction of the test waves detraps to a smaller wavenumber than to a higher wavenumber. Finally, as illustrated by taking an oceanic Richardson number of order 1 and the ratio $N/f = 75$ in figure 9, the skeleton of

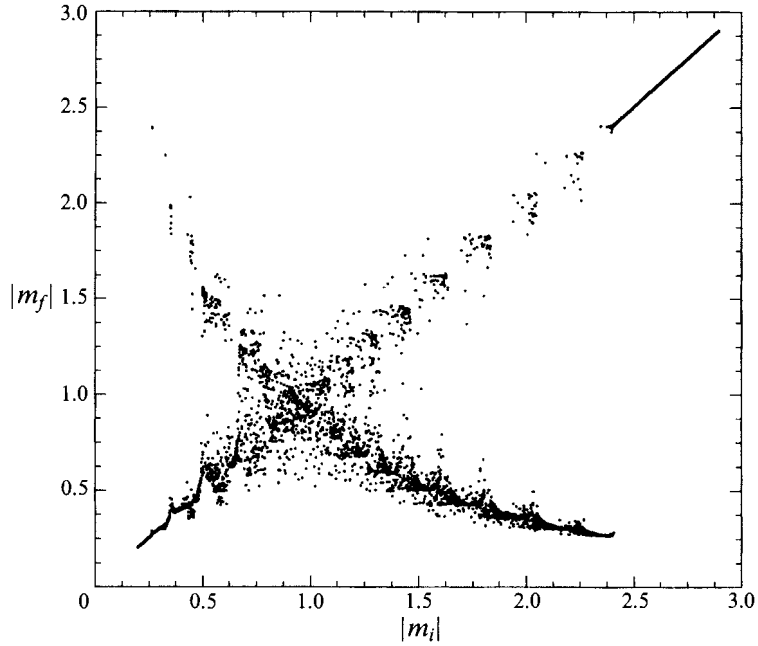

FIGURE 9. Scatter plot showing final *vs.* initial wavenumber of 5000 test waves uniformly distributed in phase obtained from simulating the full dispersion relation with $N/f = 75$. In this simulation, $\mu_0 = 2.0$ and $\varepsilon = 0.1$. Compare to figure 5(*b*).

the scattering plot is qualitatively the same as that obtained using the midfrequency approximation, and the spread of points about the skeleton looks similar. The main differences are that the scroll-like structure of the spread of points observed in the midfrequency case is seen less distinctly in figure 9 than in figure 5(*b*), and that the region of resonant wavenumbers (i.e. the range between M_a and M_b) is slightly smaller for the full dispersion relation than in the case of the midfrequency approximation. We also note that the separatrices are functionally more complicated than those we obtained using the midfrequency approximation, and therefore the quantities needed in the adiabatic separatrix crossing theory may need to be obtained numerically.

In addition to making the test wave dynamics more realistic by employing the full dispersion relation, one can also model more realistic background flows. A more realistic background flow might consist of a localized group of random waves with a very narrow spectrum, rather than a coherent wavepacket with a smooth envelope. A detailed analysis of such background flows is beyond the scope of this paper, but some general inferences can be drawn from related work in plasma physics. Graham & Fejer (1976) presented one-dimensional simulations of a charged test particle interacting resonantly with a random group of large-amplitude, infinitely long electrostatic waves, having a narrow spectrum of frequencies.

The motion of a test particle in a single electrostatic wave is identical to the motion of a plane pendulum. The coherent analogue to the Graham & Fejer wave model would be the pendulum potential in the introduction of this paper, but with an amplitude $A(\tau)$ which oscillates about some finite average value. In fact, Bruhwiler & Cary (1989) examined just such a model and found that resonant test particles repeatedly crossed the separatrix as they trapped in and subsequently de-trapped from the wave. Likewise, Graham & Fejer (1976) show phase-space trajecto-

ries of test particles that consist of three distinct regimes: (i) untrapped motion above the separatrix (i.e. particle velocity greater than mean phase velocity of the waves); (ii) untrapped motion below the separatrix (particle velocity less than wave phase velocity); and (iii) trapped motion, in which the particle executed large-amplitude oscillations around the mean phase velocity of the waves.

We are interested here in a localized wave group rather than one of infinite extent; however, the work of Graham & Fejer indicates that the fundamental phenomenon of trapping and detrapping persists as a coherent wave model is generalized to a model with some degree of randomness. Thus, there is reason to expect that the wavenumber transport observed in this paper would not be qualitatively changed by such a generalization of the near-inertial wavepacket model.

7.3. *Multiple interactions*

The problem treated in the present paper involves only a single interaction with a large-amplitude wavepacket; however, other situations may involve multiple or even periodic interactions. For wavepackets/potentials modulated periodically in the parameter λ, it is known that the region in phase space swept out by the slowly varying separatrices is chaotic. Test waves/particles wander in an apparently stochastic fashion throughout this region, with any stable islands being tiny. Menyuk (1985) provided the first numerical evidence for this picture by simulating an ensemble of test particles slowly trapping and detrapping in a single standing wave. See Elskens & Escande (1991) and Kaper & Wiggins (1991) for the general theory, and see Kaper & Wiggins (1993) for an application to a time-dependent, two-dimensional mixing study. Kaper & Wiggins (1993) show that the region in which most of the mixing and stretching occurs is the separatrix- swept region.

Both Bruhwiler & Cary (1989) and Bruhwiler & Cary (1994) study the dynamics of test particles trapping and detrapping in (i) a slowly modulated, large-amplitude single wave, and (ii) a series of broad, large-amplitude localized wavepackets. This work showed that an initial ensemble will evolve dramatically during the first few separatrix crossings, and subsequently will diffuse until it is uniformly distributed (in a coarse-grained sense) throughout the action-angle phase plane. Since there exists a canonical (i.e. area-preserving) transformation from the initial coordinate and canonical momentum to the action and its canonically conjugate angle, the diffusing ensemble also becomes uniformly distributed throughout the position–momentum phase plane. For example, if we placed the near-inertial wavepacket in a vertical one-dimensional box and forced an ensemble of high-frequency internal waves to interact repeatedly with this wavepacket, then the ensemble would eventually become uniformly distributed in the $\xi - \tilde{\omega}$ phase plane. In other words, if one were to make a profile for this situation that is analogous to the profile of the model in this paper presented in figure 8 (although we remind the reader that here the system is periodic, while in our model it is not), one would see that the spectrum is perfectly flat throughout the resonant frequency region.

We are fortunate that Bill Young suggested this problem to us several years ago. In addition, we thank him for his continuing advice. We also thank: Darryl Holm for his advice; Isidoro Orlanski for several suggestions, in particular the idea of making figure 8; the organizers of the 1990 Colorado Days meeting; and two anonymous referees for their careful reading of the paper. D. B. gratefully acknowledges partial financial support from the Grumman Corporation. T. K. gratefully acknowledges

partial financial support from the National Science Foundation through grant number MCS-9307074.

REFERENCES

BROUTMAN, D. & GRIMSHAW, R. 1988 The energetics of the interaction of short, small-amplitude internal waves and inertial waves. *J. Fluid Mech.* **196**, 93–106.

BROUTMAN, D. & YOUNG, W. R. 1986 On the interaction of small-scale oceanic internal waves with near-inertial waves. *J. Fluid Mech.* **166**, 341–358 (referred to herein as B&Y).

BRUHWILER, D. L. 1990 Scattering and diffusion of particles in slowly-varying, large-amplitude waves. PhD thesis, University of Colorado, Boulder.

BRUHWILER, D. L. & CARY, J. R. 1989 Diffusion of particles in a slowly-modulated wave. *Physica* D **40**, 265–282.

BRUHWILER, D. L. & CARY, J. R. 1992 Particle dynamics in a large-amplitude wave packet. *Phys. Rev. Lett.* **68**, 255–258.

BRUHWILER, D. L. & CARY, J. R. 1994 Dynamics of particles trapping and detrapping in coherent wave packets. *Phys. Rev.* E **50**, 3949–3961.

BYRD, P. F. & FRIEDMAN, M. D. 1954 *Handbook of Elliptic Integrals for Engineers and Physicists*, pp. 9–10. Springer.

CARY, J. R., ESCANDE, D. F. & TENNYSON, J. L. 1986 Adiabatic invariant change due to separatrix crossing. *Phys. Rev.* A **34**, 4256–4275.

CARY, J. R. & SKODJE, R. 1989 Phase change between separatrix crossings. *Physica* D **36**, 287–316.

DRUMMOND, W. E. & PINES, D. 1964 Nonlinear plasma oscillations. *Ann. Phys.* **28**, 478–499.

ELSKENS, Y. & ESCANDE, D. F. 1991 Slowly pulsating separatrices sweep homoclinic tangles where islands must be small: an extension of classical adiabatic theory. *Nonlinearity* **4**, 615–667.

FUCHS, V., KRAPCHEV, V., RAM, A. & BERS, A. 1985 Diffusion of electrons by coherent wavepackets. *Physica* D **14**, 141–160.

GRAHAM, K. N. & FEJER, J. A. 1976 One-dimensional numerical study of charged particle trajectories in turbulent electrostatic wave fields. *Phys. Fluids* **19**, 1054–1058.

HENRARD, J. 1982 Capture into resonance: an extension of the use of adiabatic invariants. *Celest. Mech.* **27**, 3–22.

HENRARD, J. 1993 The adiabatic invariant in classical mechanics. *Dynamics Reported* **2**, New Series, 117–236.

HENYEY, F. S. & POMPHREY, N. 1983 Eikonal description of internal wave interactions: a non-diffusive picture of "induced diffusion." *Dyn. Atm. Oceans* **7**, 189–219.

KAPER, T. J. & KOVAČIČ, G. 1994 A geometric criterion for adiabatic chaos. *J. Math. Phys.* **35**, 1202–1219.

KAPER, T. J. & WIGGINS, S. 1991 Lobe area in adiabatic Hamiltonian systems. *Physica* D **51**, 205–212.

KAPER, T. J. & WIGGINS, S. 1993 An analytical study of transport in Stokes flows exhibiting large-scale chaos in the eccentric journal bearing. *J. Fluid Mech.* **253**, 211–243.

KRUSKAL, M. 1962 Asymptotic theory of Hamiltonian and other systems with all solutions nearly periodic. *J. Math. Phys.* **3**, 806–828.

MCCOMAS, C. H. & BRETHERTON, F. P. 1977 Resonant interaction of oceanic internal waves. *J. Geophys. Res.* **82**, 1397–1422.

MARMORINO, G. O., ROSENBLUM, L. J. & TRUMP, C. L. 1987 Fine-scale temperature variability: the influence of near-inertial waves. *J. Geophys. Res.* **92** (C12), 13049–13062.

MEIBURG, E. & NEWTON, P. K. 1991 Particle dynamics and mixing in a viscously decaying shear layer. *J. Fluid Mech.* **227**, 211–244.

MEISS, J. D. & WATSON, K. M. 1982 Internal wave interactions in the induced-diffusion approximation. *J. Fluid Mech.* **117**, 315–341.

MENYUK, C. R. 1985 Particle motion in the field of a modulated wave. *Phys. Rev.* A **31**, 3282–3290.

MORA, P. 1992 Particle acceleration in a relativistic wave in the adiabatic regime. *Phys. Fluids* B **4**, 1630–1634.

MUNK, W. H. 1981 Internal waves and small-scale processes. In *Evolution of Physical Oceanography* (ed. B.A. Warren & C. Wunsch) p. 623. MIT Press.

NEISHTADT, A. I. 1975 Passage through a separatrix in a resonance problem with a slowly-varying parameter. *Prikl. Matem. Mekhan.* **39**, 621–632.

NEISHTADT, A. I. 1986 Change in adiabatic invariant at a separatrix. *Sov. J. Plasma Phys.* **12**, 568–573; Erratum: *Sov. J. Plasma Phys.* **13**, 441.

PERCIVAL, I. & RICHARDS, D. 1982 *Introduction to Dynamics*, Chapter 6, Cambridge University Press.

PINKEL, R. 1983 Doppler sonar observations of internal waves: wavefield structure. *J. Phys. Oceanogr.* **13**, 804–815.

ROBINSON, C. 1983 Sustained resonance for a nonlinear system with slowly-varying coefficients. *SIAM J. Math. Anal.* **14**, 847–860.

YODER, C. F. 1979 Diagrammatic theory of transition in pendulum like systems. *Celest. Mech.* **19**, 3–29.